

# Long time fully nonlinear simulation of floating body motions with artificial damping zone.

Katsuji TANIZAWA \*

## Summary

For long time simulation of floating body motions, an artificial damping zone is applied to satisfy radiation condition at the end of numerical wave tank. This artificial damping zone works as a efficient absorber of fully nonlinear waves at the tank end. Combination of this artificial damping zone and wave maker works as a absorbing wave maker. The implementation, the characteristic and the efficiency of this artificial damping zone is reported.

Using the damping zone as a wave absorber and an absorbing wave maker, a moored two dimensional body motions in regular waves are simulated by the fully nonlinear simulation method based on the velocity and acceleration potential theories <sup>4)</sup>. The simulated body motions, wave periodic motions and slow drift motion, are presented in comparison with measured motions in wave basin. The simulated motions show good correspondence with the measured motions in overall.

For the simulation of wave periodic motions of body, a numerical technique to accelerate convergence of the simulation is also given.

---

\* Ship Research Institute, Shinkawa, Mitaka, Tokyo, Japan

# 1 Introduction

Responses of floating body to incident waves are one of the main concern in ocean engineering. Linear theories and linear numerical methods are usually used as practical tools to estimate frequency responses. In the frame work of linear theory, higher order responses are analyzed by perturbation method.

Another approach to this problem is time domain nonlinear simulation. Fully nonlinear time domain simulation methods are studied by Vinje <sup>1)</sup>, Cointe <sup>2)</sup>, Tanizawa <sup>3, 4)</sup>, Kang <sup>5)</sup>, Van Daalen <sup>6)</sup>, Sen <sup>7)</sup>, Cao <sup>8)</sup> and other researchers in the past decade and many simulation programs were developed.

Time domain methods are powerful tool to simulate nonlinear response of floating body including transient phenomenon. Periodically steady body motions can be obtained as a convergent result. Higher order responses are given as Fourier components of the simulated result. To get periodically steady body motions by long time simulation, the radiation condition must be satisfied at the end of numerical wave tank.

There are roughly two choice. One is an idea to apply Sommerfeld radiation condition at the end of wave tank. This idea was taken by Orlanski <sup>9)</sup> and others <sup>10, 11, 12, 15, 14)</sup> and called as Sommerfeld-Orlanski method. Another is an idea to apply artificial damping on the free surface near the end of wave tank <sup>2, 13, 16)</sup> and called as artificial damping or sponge layer method. Sommerfeld-Orlanski radiation condition is applied at the end of wave tank and does not require additional tank length to absorb incident waves. This is a advantage of Sommerfeld-Orlanski method. This method effectively works for linear waves, but can not avoid the reflection of nonlinear component of waves when wave is steep. On the other hand, artificial damping method requires additional tank length for damping zone. But this method effectively works also for steep waves and has flexibility to use with wave maker to compose absorbing wave maker.

In this study, the artificial damping method is chosen for the simulation of two dimensional moored body motions in regular waves. The fully nonlinear simulation method based on the velocity and acceleration potential theories <sup>4)</sup> are used. The capability of this simulation method with artificial damping is discussed.

## 2 Mathematical formulation of the problem

Motions of a floating body inside a two dimensional wave basin is considered. As Fig.1 shows, fluid domain  $\Omega$  is bounded by free surfaces  $S_f$ , a piston wave maker  $S_p$ , bottom and rigid wall  $S_b$  and a floating body  $S_s$ . Here, gravitational acceleration  $g$ , density of fluid  $\rho$  and width of floating body  $B$  are chosen as units to nondimensionalize the problem. An space-fixed Cartesian coordinate system  $o-xz$  is used with  $x$  coincident with the calm free surface and  $z$  positive upward. The fluid is assumed to be homogeneous, incompressible, inviscid and its motion irrotational. The fluid motion can be described by a velocity potential  $\phi$  and its time derivative  $\phi_t$ . In the fluid domain  $\Omega$ ,  $\phi$  and  $\phi_t$  satisfies Laplace's equation

$$\nabla^2\phi = \nabla^2\phi_t = 0 . \quad (1)$$

Green's second identity can be applied on  $\phi$  and  $\phi_t$

$$c(\mathcal{Q}) \left\{ \begin{array}{l} \phi(\mathcal{Q}) \\ \phi_t(\mathcal{Q}) \end{array} \right\} = \int_S \left\{ \begin{array}{l} \phi(\mathcal{P}) \\ \phi_t(\mathcal{P}) \end{array} \right\} \frac{\partial}{\partial n} \ln r(\mathcal{P}, \mathcal{Q}) - \ln r(\mathcal{P}, \mathcal{Q}) \left\{ \begin{array}{l} \frac{\partial \phi(\mathcal{P})}{\partial n} \\ \frac{\partial \phi_t(\mathcal{P})}{\partial n} \end{array} \right\} dS, \quad (2)$$

where  $\mathcal{P}, \mathcal{Q}$  are points on the boundary,  $n$  is outward normal direction of the boundary,  $r(\mathcal{P}, \mathcal{Q})$  is distance between  $\mathcal{P}$  and  $\mathcal{Q}$ ,  $c(\mathcal{Q})$  represents the angle subtended at  $\mathcal{Q}$  by boundaries.

On the free surface, kinematic boundary condition and dynamic boundary condition for zero atmospheric pressure are applied as

$$\frac{D\phi}{Dt} = -z + \frac{1}{2}(\nabla\phi)^2 \quad (3)$$

$$\frac{D\mathbf{x}}{Dt} = \nabla\phi, \quad (4)$$

where  $\mathbf{x} = (x, z)$ . On the body surface, impermeability condition with respect to  $\phi$  is expressed as

$$\frac{\partial \phi}{\partial n} = V_n, \quad (5)$$

where  $V_n$  denotes the normal velocity of body surface. Denoting the translating and angular velocity of the body as  $\mathbf{v}_0$  and  $\boldsymbol{\omega}$  respectively,  $V_n$  is written as

$$V_n = \mathbf{n} \cdot (\mathbf{v}_0 + \boldsymbol{\omega} \times \mathbf{r}). \quad (6)$$

Impermeability condition on the body with respect to  $\phi_t$  <sup>4)</sup> is expressed as

$$\begin{aligned} \frac{\partial \phi_t}{\partial n} = & -k_n (\nabla\phi - \mathbf{v}_o - \boldsymbol{\omega} \times \mathbf{r})^2 + \mathbf{n} \cdot (\dot{\mathbf{v}}_o + \dot{\boldsymbol{\omega}} \times \mathbf{r}) \\ & + \mathbf{n} \cdot \boldsymbol{\omega} \times (\boldsymbol{\omega} \times \mathbf{r}) + \mathbf{n} \cdot 2\boldsymbol{\omega} \times (\nabla\phi - \mathbf{v}_o - \boldsymbol{\omega} \times \mathbf{r}) - \frac{\partial}{\partial n} \left( \frac{1}{2}(\nabla\phi)^2 \right), \end{aligned} \quad (7)$$

where  $k_n$  is curvature of body,  $\dot{\mathbf{v}}_o, \dot{\boldsymbol{\omega}}$  are translating and angular acceleration of body respectively.

On the floating body surface,  $\dot{\mathbf{v}}_o, \dot{\boldsymbol{\omega}}$  can not be specified explicitly and implicit boundary condition should be applied. Denoting the inertia tensor of the floating body as  $\mathcal{M}$  and generalized normal vector of body surface as  $\mathbf{N} = (\mathbf{n}, \mathbf{n} \times \mathbf{r})$ , the implicit boundary condition is written as

$$\begin{aligned} \frac{\partial \phi_t}{\partial n} = & \mathbf{N} \mathcal{M}^{-1} \left\{ \int_{S_s} -\phi_t \mathbf{N} ds \right\} \\ & + \mathbf{N} \mathcal{M}^{-1} \left\{ \int_{S_s} \left( -z - \frac{1}{2}(\nabla\phi)^2 \right) \mathbf{N} ds + \mathbf{F}_g \right\} \\ & + q - \frac{\partial}{\partial n} \left( \frac{1}{2}(\nabla\phi)^2 \right), \end{aligned} \quad (8)$$

where  $\mathbf{F}_g$  is sum of gravity, mooring force and other external forces acts to the body and  $q$  is the term which can be explicitly evaluated from the solution of velocity field as

$$\begin{aligned} q = & -k_n (\nabla\phi - \mathbf{v}_o - \boldsymbol{\omega} \times \mathbf{r})^2 \\ & + \mathbf{n} \cdot \boldsymbol{\omega} \times (\boldsymbol{\omega} \times \mathbf{r}) + \mathbf{n} \cdot 2\boldsymbol{\omega} \times (\nabla\phi - \mathbf{v}_o - \boldsymbol{\omega} \times \mathbf{r}). \end{aligned} \quad (9)$$

With these boundary conditions and Green's second identity with respect to  $\phi$  and  $\phi_t$ , velocity field and acceleration field can be solved numerically. The solutions are numerically integrated with respect to time to simulate the problem in time domain. In this paper, boundary value problems on  $\phi$  and  $\phi_t$  are solved by BEM, 4th order Runge-Kutta method is used for time integral and MEL <sup>17)</sup> is used to update free surface.

### 3 Artificial damping zone

#### 3.1 Implementation of damping zone

Following a preceding work of Cointe et al. <sup>2)</sup>, damping terms are added to dynamic and kinematic free surface boundary conditions to give artificial damping effect to free surface. The free surface boundary conditions are given as

$$\frac{D\phi}{Dt} = -z + \frac{1}{2}(\nabla\phi)^2 - \nu(x_\epsilon)(\phi - \phi_\epsilon) \quad (10)$$

$$\frac{D\mathbf{x}}{dt} = \nabla\phi - \nu(x_\epsilon)(\mathbf{x} - \mathbf{x}_\epsilon) . \quad (11)$$

where  $\nu(x_\epsilon)$  is the damping coefficient

$$\nu(x) = \begin{cases} \alpha\omega\left(\frac{x-x_0}{\lambda}\right)^2, & \text{for } x_0 \leq x \leq x_1 = x_0 + \beta\lambda \\ 0, & \text{for } x < x_0 \text{ or } x > x_1 \end{cases} . \quad (12)$$

In the definition of  $\nu(x)$ ,  $\omega$  and  $\lambda$  are angular frequency and wave length of the incident wave respectively. The characteristic of this damping zone is controlled by two nondimensional parameter  $\alpha$  and  $\beta$ .  $\alpha$  is used to control the strength of damping and  $\beta$  is used to control the length of damping zone.  $\phi_\epsilon, \mathbf{x}_\epsilon$  are reference values. This damping zone damp down differences  $\phi - \phi_\epsilon$  and  $\mathbf{x} - \mathbf{x}_\epsilon$ . As Fig.2 shows, when the damping zone work as a simple absorber, the reference values are set to  $\phi_\epsilon = 0, \mathbf{x}_\epsilon = (x_\epsilon, 0)$ . And as Fig.3 shows, when the damping zone is combined with wave maker and works as an absorbing wave maker,  $\phi_\epsilon$  and  $\mathbf{x}_\epsilon$  are given from a wave simulation without bodies in the tank. For practical purpose, linear analytical solution can be a good substitution of  $\phi_\epsilon$  and  $\mathbf{x}_\epsilon$ . For piston wave maker, linear propagating wave is described as

$$\phi(x, z, t) = \frac{4s \tanh kh \sinh kh}{\omega(2kh + \sinh 2kh)} \cosh k(z+h) \cos(kx - \omega t) \quad (13)$$

$$\eta(x, t) = -\left. \frac{\partial\phi}{\partial t} \right|_{z=0} = \frac{4s \sinh^2 kh}{2kh + \sinh 2kh} \sin(kx - \omega t) \quad (14)$$

where  $s$  is stroke of the wave maker and  $k$  is wave number of the generated wave. Numerical example of absorbing wave maker with these analytical solutions are given in section 3.2.2.

#### 3.2 Performance of the damping zone

##### 3.2.1 Wave absorption efficiency

Wave absorption efficiency of the damping zone is studied. Fig.5 shows wave profiles of periodically steady state inside and outside of the damping zone at  $t = 45T_w, 45.25T_w, 45.5T_w$  and  $45.75T_w$ , where  $T_w$  is wave period. Wave slope of the incident wave is about  $1/25$  in this case. For this simulation, both  $\alpha$  and  $\beta$  are set to 1. Wave damping inside the damping zone is clearly observed in this figure.

Quantitative evaluation of the wave absorption efficiency can be done by computing the wave reflection coefficient. Roughly two methods are known to estimate reflection coefficient of real test basin. One method uses a wave probe with constant forward velocity. The reflection coefficient is estimated using the difference of encounter frequency of incident and reflected waves. Another

method uses two fixed wave probes to separate incident wave and reflected wave from measured data. This method is known as Goda's method <sup>18)</sup>, see Appendix A. Since the exact reflection coefficient of nonlinear wave is difficult to obtained, Goda's method is used to get estimation.  $\zeta_1, \zeta_2$  in Fig.6 are simulated wave elevation at  $x_1 = 3.00, x_2 = 3.05$  in the simulation of Fig.5.  $a_I$  and  $a_R$  are amplitude of incident wave and reflected wave estimated by Goda's method and  $a_R/a_I$  is the reflection coefficient. After transient phenomenon decayed ( $t > 10T_w$ ), the reflection coefficient converges to a constant value, 1.8%.

Wave absorption efficiency of the damping zone is a function of  $\alpha$  and  $\beta$ . Fig.7 shows the relation between reflection coefficient and  $\alpha$  when  $\beta = 1$ . At  $\alpha = 0$ , no damping is applied. As  $\alpha$  becomes larger, the reflection coefficient becomes smaller and reaches to minimum value at  $\alpha \approx 1$ . For larger  $\alpha$ , the reflection coefficient rises gradually. Next, Fig.8 shows the relation between reflection coefficient and  $\beta$  when  $\alpha = 1$ . At  $\beta = 0$ , length of the damping zone is zero and neither damping is applied. As  $\beta$  becomes larger, the reflection coefficient becomes smaller and reaches to minimum and steady value at  $\beta \approx 1$ . This figure shows one wave length of damping zone is efficient enough. From above argument,  $\alpha = \beta = 1$  is the appropriate combination of tuning parameter of the damping zone.

Dependency of the wave absorption efficiency to wave steepness is plotted in Fig.9. Reflection coefficient of entire damping zone is plotted with solid line and white circle. When wave slope becomes steeper, estimated reflection coefficient by Goda's method is slightly larger, but still less than 3% and energy reflection coefficient is less than 1/1000. In general, this level of reflection is smaller than that of wave absorbing beach of real test basin and acceptable for numerical simulation.

The solid line with black circle in Fig.9 is the reflection coefficient only from the tank end. This value is estimated from the incident wave amplitude  $a_I$  and standing wave amplitude on the vertical wall of the tank end  $a_S$ . Since the wave amplitude at the tank end is a half of  $a_S$ , wave damping coefficient is roughly given as  $a_S/2a_I$ . Taking that damping is effective not only incident wave but also reflected wave from the tank end, the reflection coefficient from the tank end can be roughly estimated by  $(a_S/2a_I)^2$ . Compare with the total reflection from the damping zone, reflection from the tank end is insignificant.

### 3.2.2 Absorbing wave maker

As shown in Fig.3, an absorbing wave maker is composed of a piston wave maker and a damping zone with analytical reference values given by Eq.(13,14). The parameters of the damping zone is set to  $\alpha = \beta = 1$ .

First, simulated wave profiles at  $t = 4T_w, 4.25T_w, 4.5T_w$  and  $4.75T_w$  are plotted in Fig.10. Solid lines show simulated wave profiles with damping zone and dashed lines show those of without damping zone. Stroke of the wave maker  $s$  is controlled as

$$s(t) = \begin{cases} st/T_w, & \text{for } 0 \leq t < T_w \\ s, & \text{for } t \geq T_w \end{cases} \quad (15)$$

so that generated wave will not break in front of the wave maker when the wave make begin to move. While the gradual start up of wave maker  $0 \leq t < T_w$ , no wave damping is applied.

Compare with the dashed lines, the amplitude of solid lines are a little lower and slight difference can be observed in the front shape of the wave. The damping zone with analytical reference values may not be applicable to exact wave simulation. But, this absorbing wave maker is useful for nonlinear simulation of floating body motions.

To show the wave absorption performance, the amplitude of wave at  $x = 3$  is plotted in Fig.11. This figure shows that the generated wave reaches the point  $x = 3$  at  $t \approx 7T_w$ , the reflected wave from the tank end reaches at  $t \approx 17T_w$  and the wave amplitude keeps constant for  $t > 17T_w$ . Almost no wave is reflected from the absorbing wave maker. Quantitative estimation of the reflection coefficient of this absorbing wave maker is hard, but it is considered to be small enough for practical use.

## 4 Simulation of a floating body motions with damping zones

Using the numerical wave tank shown in Fig.4, a floating body motions are simulated. The body is moored by weak and linear spring in horizontal direction to restrict free drifting. Fig.14 and Table 1 show the body shape and principal dimensions. Two regular waves, Wave.1 ( $\lambda/B = 3.65, 2\zeta_a/\lambda \approx 1/32$ ) and Wave.2 ( $\lambda/B = 2.43, 2\zeta_a/\lambda \approx 1/15$ ) are used for the simulation.

First, simulated body motions for 50 wave periods in Wave.1 are presented in Fig.12. The horizontal motion has swaying and slow drifting component caused by wave drift force and restoring force of the mooring. The swaying amplitude converges to a constant value quickly, while the slow drift motion decays gradually and converges to the balancing position of the restoring force with the steady wave drift force. Heave is affected little by the horizontal motions and converges to the periodically steady state faster than others. Roll is affected some by the horizontal motions but nearly converges to the periodically steady state with heel angle to the lee side at the end of the simulation.

Next, simulated body motions for 50 wave periods in Wave.2 are presented in Fig.13. Wave.2 is shorter and steeper than Wave.1. In this case, slow drift damping is weak and amplitude of slow drift motion is large. The influence of slow drift motion can be observed both heave and roll motions. Longer simulation is required to get periodically converged result in Wave.2.

To validate these simulations, measured motions in Wave.1 and Wave.2 are presented in Fig.16 and Fig.17 respectively. The experiment was conducted in two dimensional portable wave channel installed in the seakeeping test basin of Ship Research Institute, see Fig.15. Two dimensionality is roughly kept inside of short channel. The incident wave was generated by the flap wave maker. Since this wave maker is not absorbing type, valid measuring time is limited.

The overall correspondence between simulation and experiment in Wave.1 is very good. Since the slow drift damping of the horizontal motion in the experiment is slightly weak, the drift motion affects to heave and roll motion a little. The disturbance at the tail of measured motions are effect of the reflected wave. The simulated motions, the first order response and the second order response, show in good agreement with the measured motions.

On the other hand, the correspondence between simulation and experiment in Wave.2 is not as good as in Wave.1. In particular, the significant difference can be observed in the slow drift

motion. The slow drift damping of measured motion is strong while that of simulation is weak. This difference affects not only horizontal motion but also heave and roll motions. Simulated heave and roll motions are affected by the large drift motion and convergence is slow. One possible reason of the difference is viscous damping. Resonance between slow drift motion and entire numerical wave tank can be another possible reason. As this simulation shows, the second order motion strongly affects to the first order motions. In fully nonlinear simulation, we can not separate the first order solution from higher order solution. Therefore accuracy of the higher order components are as important as the first order component for the fully nonlinear simulation. Further study will be needed to develop reliable numerical wave tank even for two dimensional problems.

In the simulation, the main damping force of the slow drift motion is considered to be wave drift damping by following reason. The natural period of slow drift motion  $T_{sd}$  is much longer than wave period and the length of radiation wave corresponding to period  $T_{sd}$  is about  $526B$ . Therefore damping force due to radiation of this long wave is negligible. The Kelvin waves due to slow drifting speed  $U$  can be neglected. Neither viscous effect can be a damping force, because ideal fluid is assumed in this simulation.

The Wave drift damping can be roughly estimated from the simulation as follows. Fig.18 shows simulated wave drift force  $F_x$  and drift speed  $U$ . To get  $F_x$  and  $U$ , FFT is applied to remove high frequency components from the simulated hydraulic force and velocity of the body. In the linear theory<sup>19)</sup>, wave drift damping  $B_x$  is defined as

$$B_x = - \left. \frac{\partial F_x}{\partial U} \right|_{U=0}, \quad (16)$$

where  $F_x$  and  $U$  are steady values with respect to time and  $U$  is taken positive when drifting to  $x$  direction. The simulated  $F_x$  and  $U$  in Fig.18, on the other hand, are functions of time. This is the difference between linear theory and nonlinear simulation. But if we take Eq.(16) also for nonlinear simulation,  $B_x$  is given by  $\partial F_x / \partial U$  at  $U = 0$ . The relation between  $F_x$  and  $U$ , ( $10T_w \leq t \leq 40T_w$ ) is plotted in Fig.19. The arrows show that the tangent of  $F_x$  at  $U = 0$  are negative for both Wave.1 and Wave.2 and so positive wave drift damping ( $B_x \text{ in Wave.1} > B_x \text{ in Wave.2} > 0$ ) acts to the body.

When we want to simulate the periodically steady motions of the body, the slow drift motion is an obstacle. An artificial mooring without restoring force is introduced in the simulation to remove slow drift oscillation and accelerate the convergence to the periodically steady state. The artificial mooring force is given as

$$\begin{aligned} F_m(t) &= -\bar{f}_x(t) - \frac{M}{NT_w} \bar{v}_x(t) \\ &= -\frac{1}{NT_w} \int_{t-NT_w}^t f_x(\tau) d\tau - \frac{M}{(NT_w)^2} \int_{t-NT_w}^t v_x(\tau) d\tau, \end{aligned} \quad (17)$$

where  $\bar{f}_x$  and  $\bar{v}_x$  are mean values of horizontal hydraulic force and swaying velocity in the past  $N$  wave period and  $M$  is body mass. Damping coefficient of this mooring force  $M/NT_w$  is selected so that drifting momentum tends to zero in future  $N$  wave period. When drifting speed converges to zero, no damping affects to the periodical body motions. Simulation with this artificial mooring ( $N = 2$ ) in Wave.1 is shown in Fig.20. No restoring force is included in the mooring

force and so no slow drift oscillation is observed. Sway and heave converge quickly within  $10T_w$  and roll takes  $20T_w$  to converge because of weak roll damping.  $F_m(t)$  plotted in the bottom of Fig.20 also converges quickly to the steady wave drift force.

## 5 Conclusion

An artificial damping zone is introduced and long time fully nonlinear simulation of floating body motions are conducted in regular waves. Following items are conclusion of this study.

1. The artificial damping terms added to kinematic and dynamic free surface boundary condition inside damping zone effectively work to absorb even steep waves and its reflection coefficient is small enough for practical use.
2. The artificial damping zone combined with a piston wave maker is effectively works as an absorbing wave maker. The analytical solution of the propagating wave generated by piston wave maker can be a practical substitution of the exact reference values of the damping zone.
3. Combination of the damping zone and the absorbing wave maker is useful for fully nonlinear long time simulation of floating body motions.
4. The results of long time simulation show good correspondence with the experiment in overall.
5. Simulated wave drift damping in Wave.2 dose not agree with the measured damping. Further study is needed to improve the reliability of simulation.
6. For the simulation of wave periodic motions of body, the artificial mooring without restoring force is effective to accelerate convergence of the simulation.

## References

- 1) Vinje,T. and Brevig,P.: Nonlinear Ship Motions, *Proc. of the 3rd. Int. Conf. on Num. Ship Hydro.*, ppIV3-1-IV3-10, (1981)
- 2) Cointe,R., Geyer,P., King,B., Molin,B. and Tramoni,M.: Nonlinear and linear motions of a rectangular barge in a perfect fluid, *Proc. 18th Symp. Naval Hydro.*, pp85-99, (1990)
- 3) Tanizawa,K.: A numerical method for nonlinear simulation of 2-D body motions in waves by means of B.E.M., *Journal of SNAJ*, Vol.168, pp223-228, (1990), *in Japanese*
- 4) Tanizawa,K.: A Nonlinear Simulation Method of 3-D Body Motions in Waves, *Journal of SNAJ*, Vol.178, pp179-191, (1995)
- 5) Kang,C.G. and Gong,I.Y.: A numerical solution method for three-dimensional nonlinear free surface problems, *Proc. 18th Symp. Naval Hydro.*, pp427-438, (1990)
- 6) Van Daalen,E.F.G.: Numerical and Theoretical Studies of Water Waves and Floating Bodies, *Ph.D. thesis, University of Twente, The Netherlands*,(1993)
- 7) Sen,D.: Numerical Simulation of motions of two-dimensional floating bodies, *JSR*, vol.37, No.4, pp307-330, (1993)
- 8) Cao,Y.,Beck,R. and Schultz,W.W.: Nonlinear motions of floating bodies in incident waves, *9th Workshop on Water Waves and Floating Bodies, Kuju,Oita*, pp33-37, (1994)
- 9) Orlandi,I.: A simple boundary condition for unbounded hyperbolic flows,*J. of Comp. Physics*, vol.21,(1976)
- 10) Romate,J.E.:Absorbing boundary conditions for free surface waves. *J. of Comp. Physics*, vol.99,pp135-145,(1992)
- 11) Liu,P.L-F. and Abbaspour,M.:An integral equation method for the diffraction on oblique waves by an infinite cylinder. *Int. J. of Numerical Methods in Eng. vol.18*,pp1497-1504,(1982)
- 12) Nestegard,A. and Sclavounos,P.D.:A numerical solution of two-dimensional deep water wave-body problems. *JSR, Vol.28*,pp48-54,(1984)
- 13) Chan,R.K.C.:Two dimensional time-dependent calculations of large-amplitude surface gravity waves due to a surface disturbance. *Proc. of 1st Int. Conf. on Numerical Ship Hydro.*,pp315-331,(1975)
- 14) Yen,S.M. and Hall,D.R.:Implementation of open boundary conditions for nonlinear free-surface wave problems. *Proc. of 3rd Int. Conf. on Numerical Ship Hydro.*,pp163-176,(1981)
- 15) Chan,R.K.C.:Finite difference simulation of the planar motion of a ship. *Proc. of 2nd Int. Conf. on Numerical Ship Hydro.*,pp39-52,(1977)

- 16) Baker,G.R.,Merion,D.I. and Orszag,S.A.:Application of a generalized vortex method to non-linear free-surface flows. *Proc. of 3rd Int. Conf. on Numerical Ship Hydro.*,pp179-191,(1981)
- 17) Longuet-Higgins,M.S. and Cokelet,E.: The deformation of steep surface waves on water, *Proc. Roy. Soc. ser.A350*, pp1-26, (1976)
- 18) Goda,Y., Suzuki,Y.,Kishira,Y. and Kikuchi,O. : Estimation of incident and reflected waves in random wave experiments. *Rept. Port and Harbour Res. Inst., vol.248*,pp3-24,(1976)
- 19) Sunahara,S.: Study on wave drift damping of multiple vertical cylinders, *Ph.D thesis*, The Univ. of Tokyo, (1994). (in Japanese)

## Appendix A Goda's method to estimate reflection coefficient

The abstract of Goda's method <sup>18)</sup> is described. Here we are considering a linear regular wave of wave number  $k$  and angular frequency  $\omega$ . Incident wave and reflected wave can be expressed as

$$\zeta_I = a_I \cos(kx - \omega t + \theta_I) \quad (\text{A.1})$$

$$\zeta_R = a_R \cos(kx + \omega t + \theta_I), \quad (\text{A.2})$$

where  $a_I$  and  $a_R$  are amplitude,  $\theta_I$  and  $\theta_R$  are phase of incident and reflected waves respectively. Two wave elevation simultaneously measured at two fixed points at  $x_1$  and  $x_2 = x_1 + \Delta l$  are written as

$$\zeta_1 = (\zeta_I + \zeta_R)_{x=x_1} = A_1 \cos \omega t + B_1 \sin \omega t \quad (\text{A.3})$$

$$\zeta_2 = (\zeta_I + \zeta_R)_{x=x_2} = A_2 \cos \omega t + B_2 \sin \omega t, \quad (\text{A.4})$$

where

$$\left. \begin{aligned} A_1 &= a_I \cos \phi_I + a_R \cos \phi_R \\ B_1 &= a_I \sin \phi_I - a_R \sin \phi_R \\ A_2 &= a_I \cos(k\Delta l + \phi_I) + a_R \cos(k\Delta l + \phi_R) \\ B_2 &= a_I \sin(k\Delta l + \phi_I) - a_R \sin(k\Delta l + \phi_R) \end{aligned} \right\} \quad (\text{A.5})$$

$$\left. \begin{aligned} \phi_I &= kx_1 + \theta_I \\ \phi_R &= kx_1 + \theta_R \end{aligned} \right\} . \quad (\text{A.6})$$

Four equations in (A.5) can be used to solve four unknowns  $a_I, a_R, \phi_I, \phi_R$ . The solutions are given as

$$a_I = \frac{1}{2|\sin k\Delta l|} [(A_2 - A_1 \cos k\Delta l - B_1 \sin k\Delta l)^2 + (B_2 + A_1 \sin k\Delta l - B_1 \cos k\Delta l)^2]^{\frac{1}{2}} \quad (\text{A.7})$$

$$a_R = \frac{1}{2|\sin k\Delta l|} [(A_2 - A_1 \cos k\Delta l + B_1 \sin k\Delta l)^2 + (B_2 - A_1 \sin k\Delta l - B_1 \cos k\Delta l)^2]^{\frac{1}{2}} \quad (\text{A.8})$$

$$\phi_I = \tan^{-1} \left[ \frac{-A_2 + A_1 \cos k\Delta l + B_1 \sin k\Delta l}{B_2 + A_1 \sin k\Delta l - B_1 \cos k\Delta l} \right] \quad (\text{A.9})$$

$$\phi_R = \tan^{-1} \left[ \frac{-A_2 + A_1 \cos k\Delta l - B_1 \sin k\Delta l}{-B_2 + A_1 \sin k\Delta l + B_1 \cos k\Delta l} \right]. \quad (\text{A.10})$$

$A_1, A_2, B_1, B_2$  is given from Fourier analysis of measured data  $\zeta_1, \zeta_2$ . The reflection coefficient is given as  $a_R/a_I$ .

## List of Figures

1	Geometric definition . . . . .	14
2	Damping zone as a simple wave breaker . . . . .	14
3	Damping zone as a absorbing wave maker . . . . .	14
4	Simulation with damping zones . . . . .	15
5	Wave profiles inside and outside of the damping zone, $\alpha = 1, \beta = 1, t = 45T_w, 45.25T_w, 45.5T_w$ and $45.75T_w$ ( $T_w$ : wave period) . . . . .	16
6	Reflection coefficient estimation by Goda's method . . . . .	17
7	Reflection coefficient vs. $\alpha$ . . . . .	18
8	Reflection coefficient vs. $\beta$ . . . . .	18
9	Reflection coefficient vs. $2a_I/\lambda$ . . . . .	19
10	Wave profiles inside and outside of the wave making damping zone $\alpha = 1, \beta = 1, t = 4T_w, 4.25T_w, 4.5T_w$ and $4.75T_w$ ( $T_w$ : wave period) . . . . .	20
11	Wave amplitude at $x = 3$ . . . . .	20
12	Simulated floating body motions in Wave.1 . . . . .	21
13	Simulated floating body motions in Wave.2 . . . . .	22
14	Body shape . . . . .	23
15	Two dimensional portable wave channel installed in wave tank . . . . .	23
16	Measured floating body motions in Wave.1 . . . . .	24
17	Measured floating body motions in Wave.2 . . . . .	25
18	Wave drift force and drifting speed . . . . .	26
19	Plot of wave drift force vs. drifting speed . . . . .	27
20	Simulated floating body motions with the artificial mooring . . . . .	28

## List of Tables

1	Principal dimensions of the floating body . . . . .	13
---	---	----

Table 1: Principal dimensions of the floating body

Item		M-K-S system	Nondimensional value
Breadth	$B$	0.74 m	1.0
Draft	$d$	0.25 m	0.338
Displacement	$\Delta$	184.3 kg	0.337
Center of inertia	$KG$	0.22 m	0.297
Radius of inertia	$R_I$	0.266 m	0.359
Natural period of heave	$T_h$	1.408 sec	5.12
Natural period of roll	$T_r$	1.775 sec	6.46
Spring constant of mooring	$k_m$	51.07 N/m	0.00704

Principal dimensions are nondimensionalized using breadth of body (  $B = 0.74m$  ), density of water (  $\rho = 1000kg/m^3$  ) and gravitational acceleration (  $g = 9.8m/s^2$  ) as units.

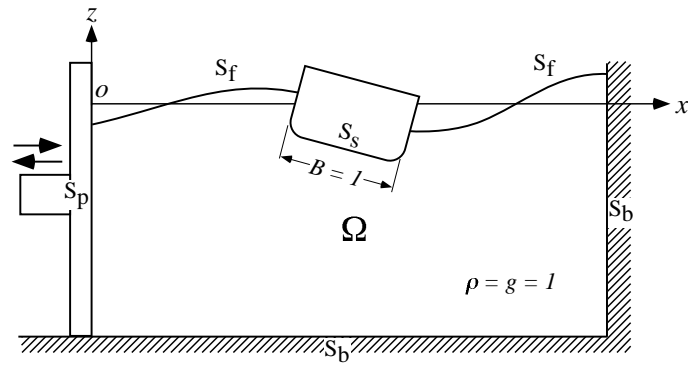


Fig.1: Geometric definition

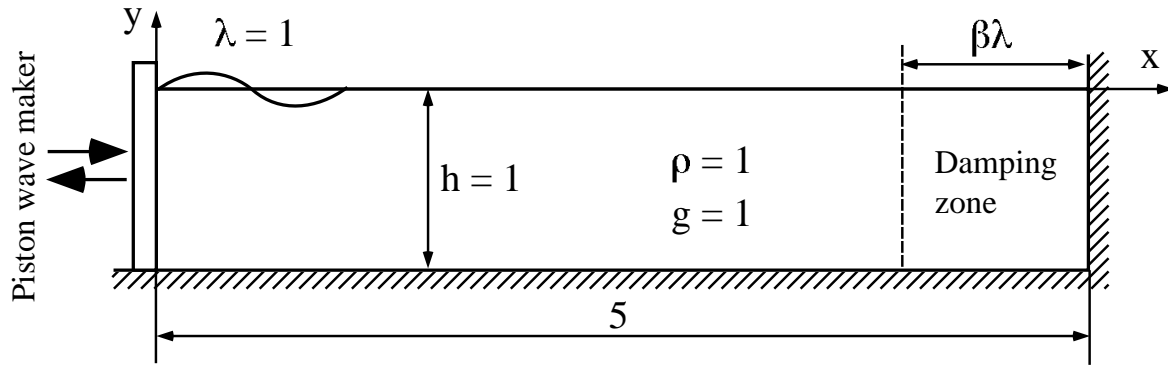


Fig.2: Damping zone as a simple wave breaker

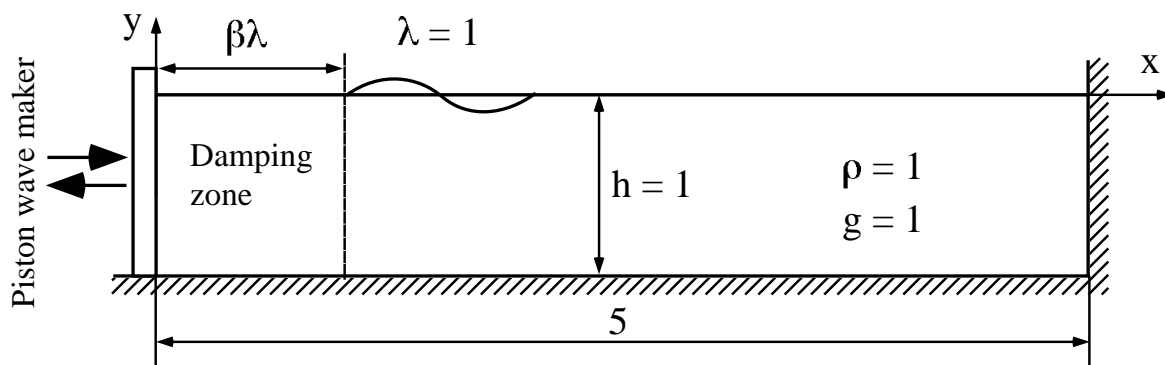


Fig.3: Damping zone as an absorbing wave maker

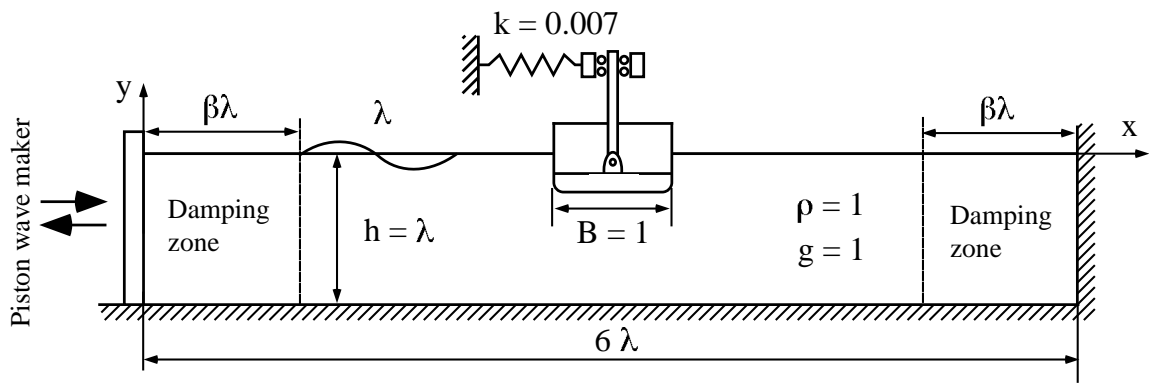


Fig.4: Simulation with damping zones

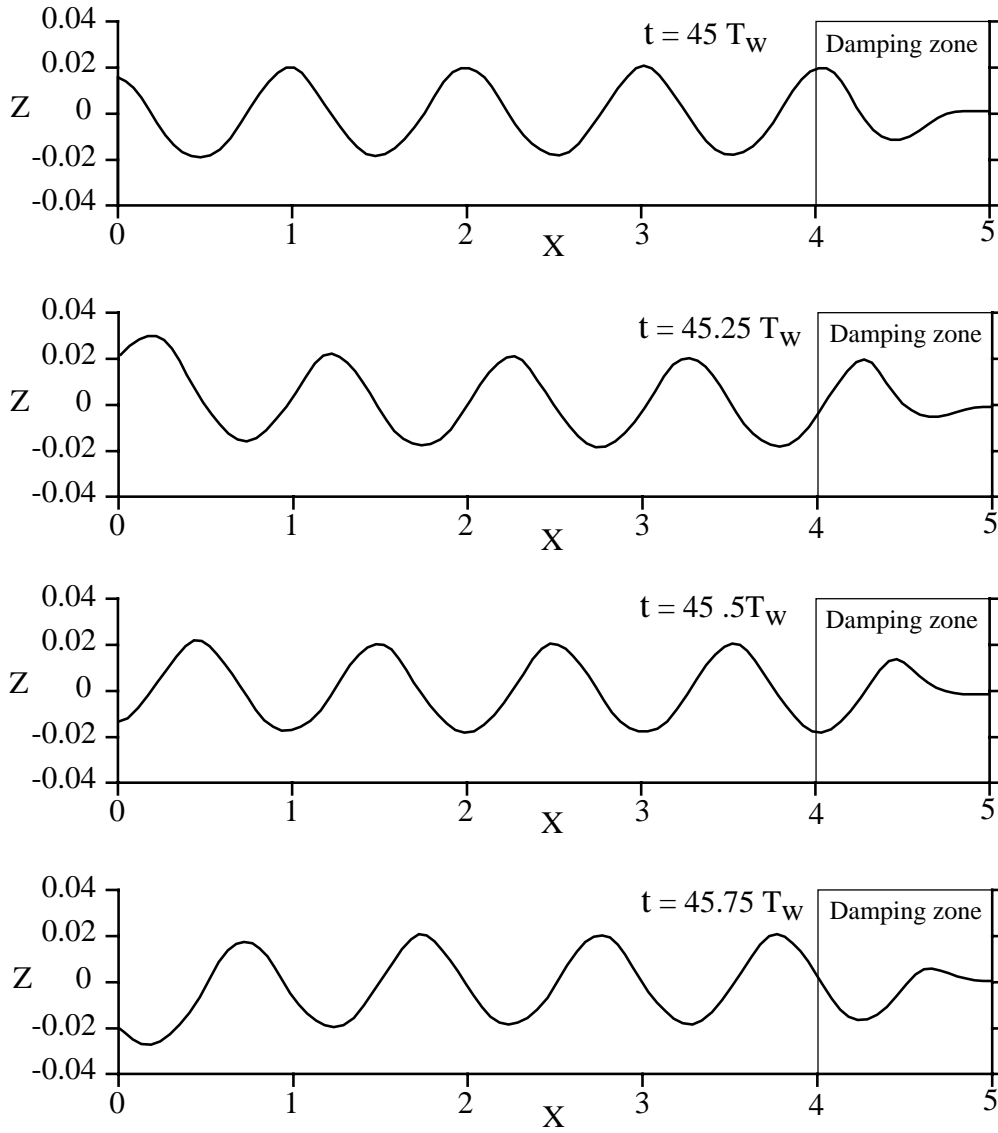


Fig.5: Wave profiles inside and outside of the damping zone,  $\alpha = 1, \beta = 1, t = 45T_w, 45.25T_w, 45.5T_w$  and  $45.75T_w$  ( $T_w$  : wave period)

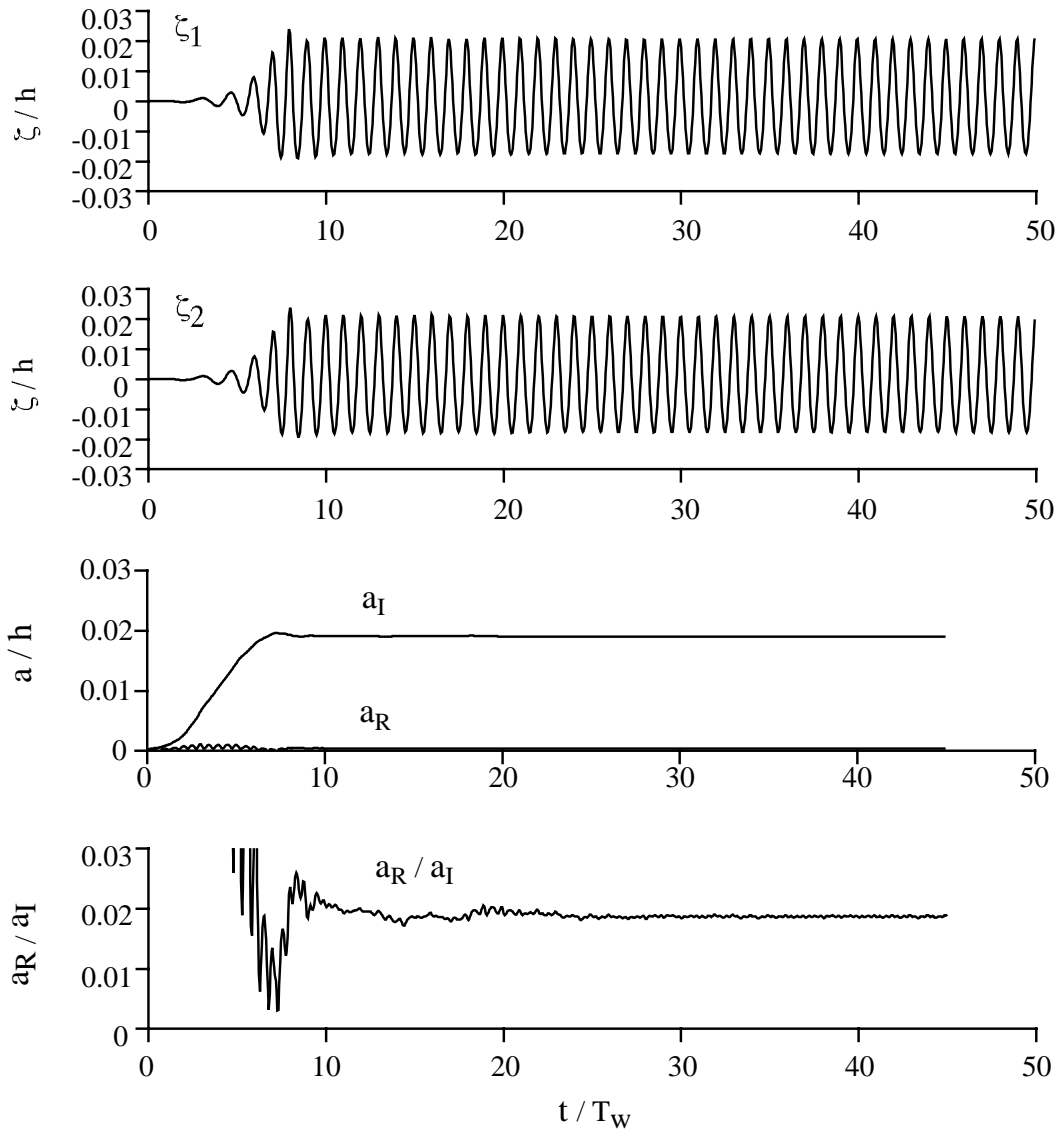


Fig.6: Reflection coefficient estimation by Goda's method

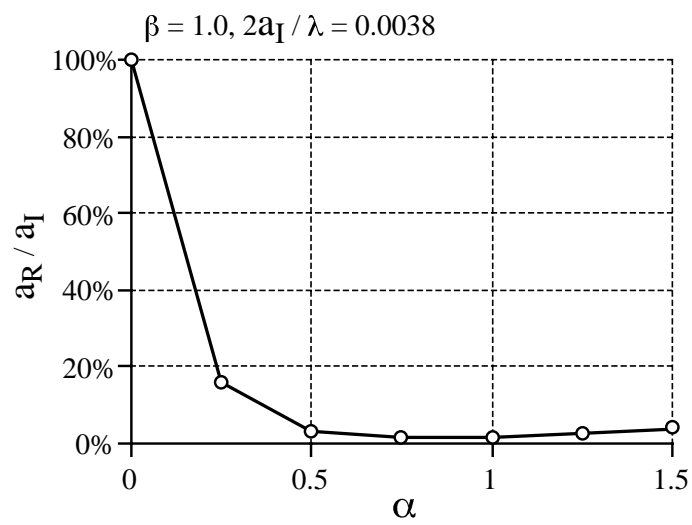


Fig.7: Reflection coefficient vs.  $\alpha$

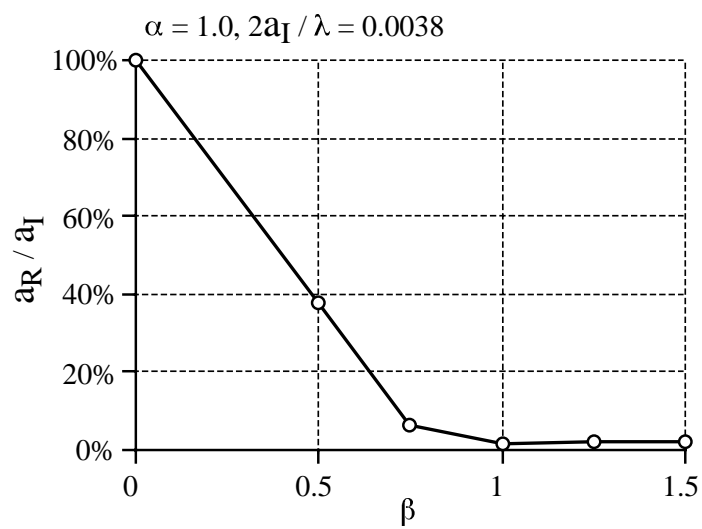


Fig.8: Reflection coefficient vs.  $\beta$

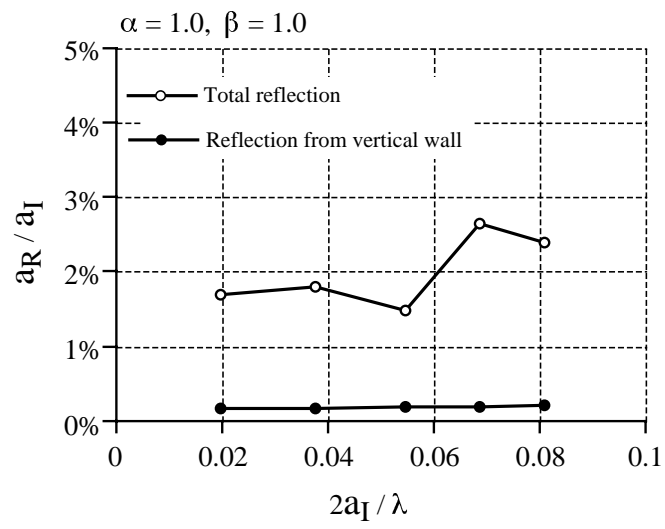


Fig.9: Reflection coefficient vs.  $2a_I/\lambda$

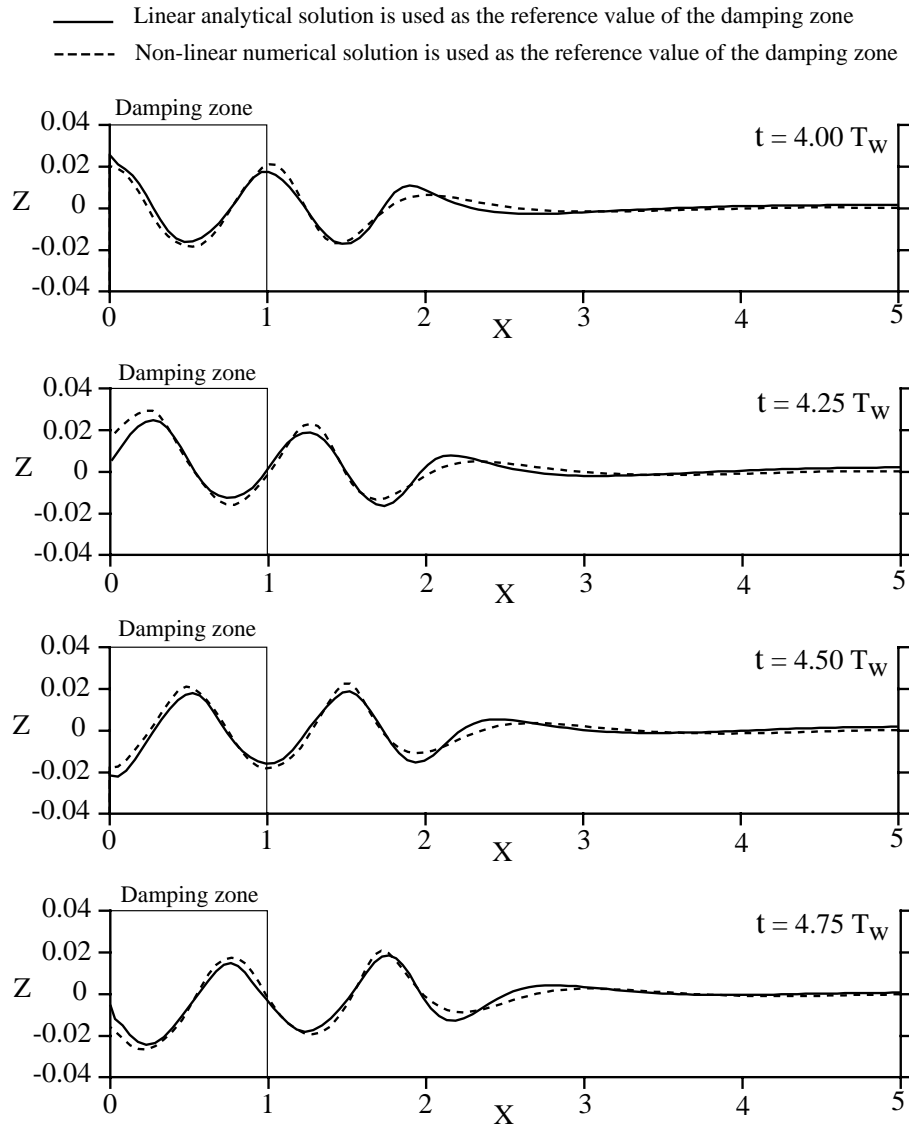


Fig.10: Wave profiles inside and outside of the wave making damping zone  $\alpha = 1, \beta = 1, t = 4T_w, 4.25T_w, 4.5T_w$  and  $4.75T_w$  ( $T_w$  : wave period)

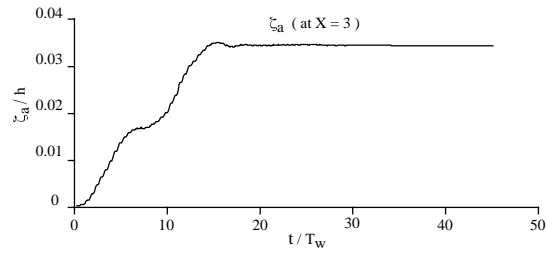


Fig.11: Wave amplitude at  $x = 3$

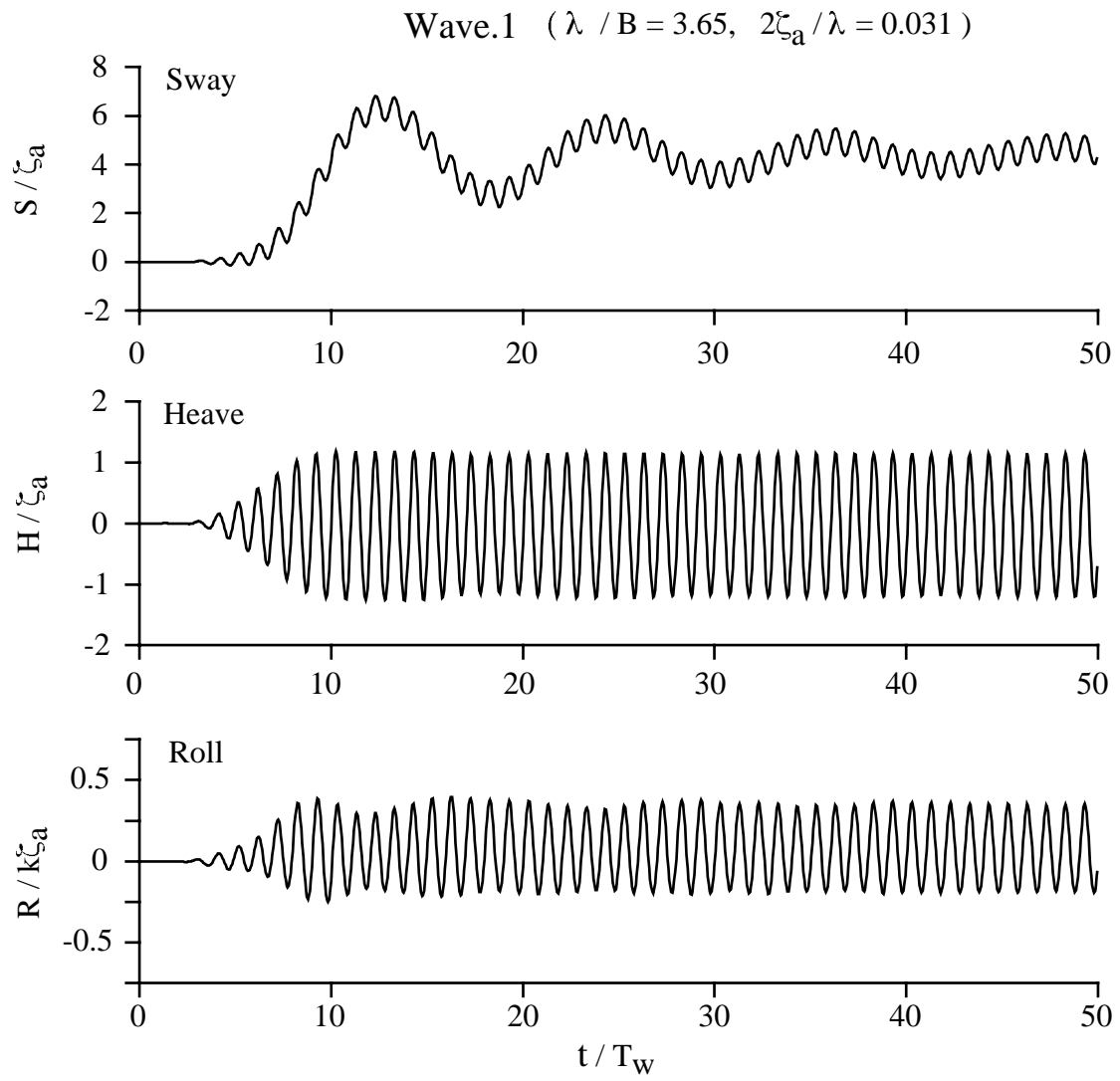


Fig.12: Simulated floating body motions in Wave.1

Wave.2 ( $\lambda / B = 2.43$ ,  $2\zeta_a / \lambda = 0.06$ )

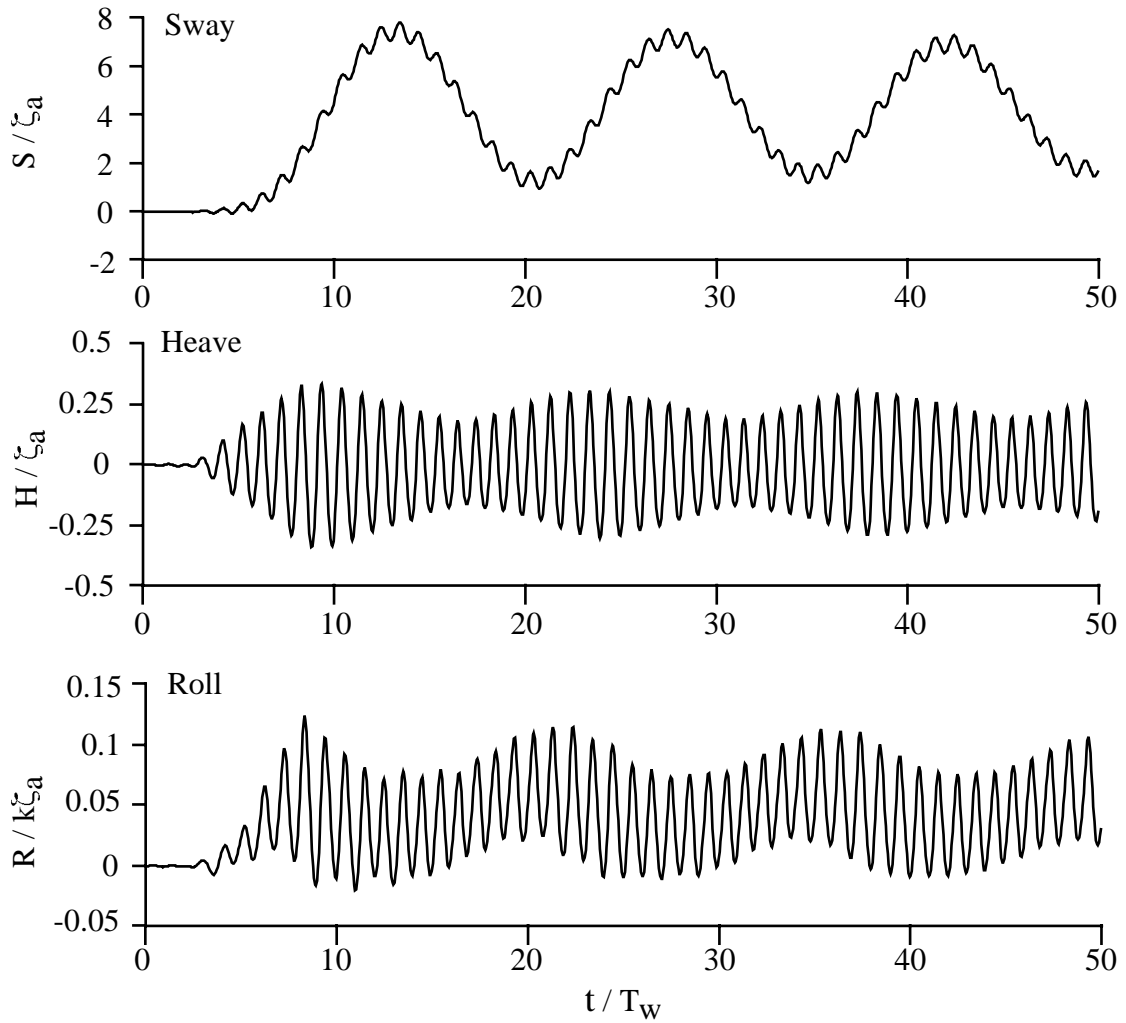


Fig.13: Simulated floating body motions in Wave.2

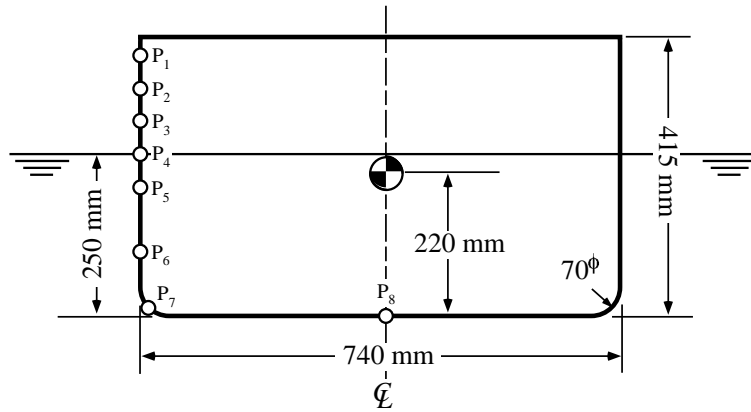


Fig.14: Body shape

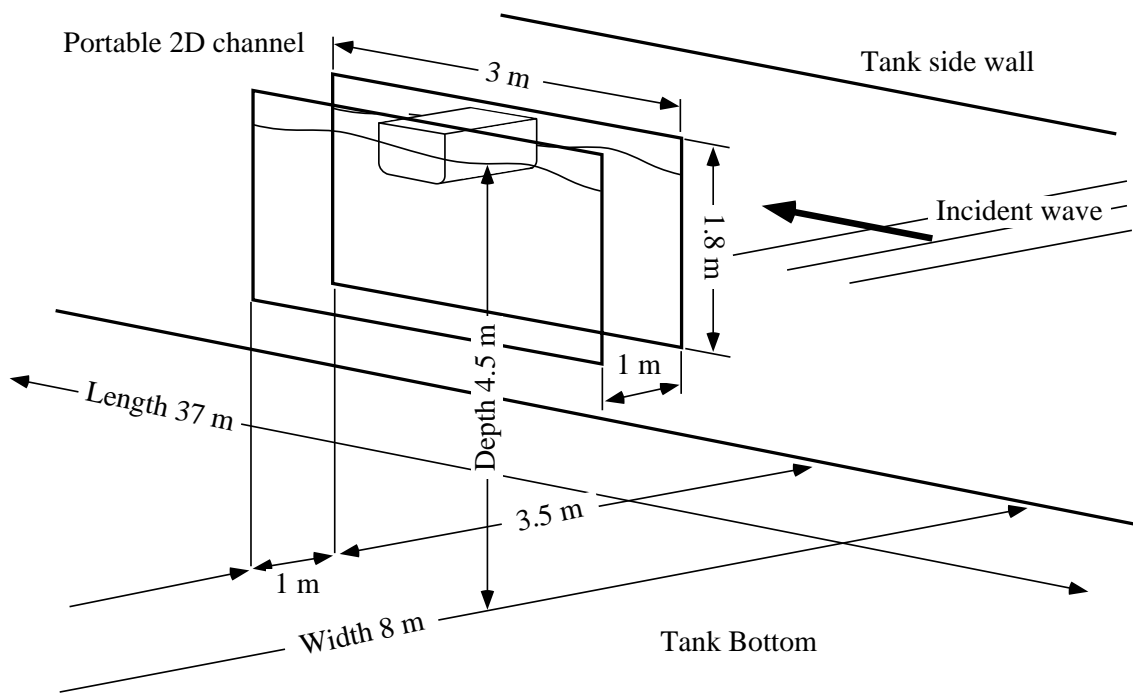


Fig.15: Two dimensional portable wave channel installed in wave tank

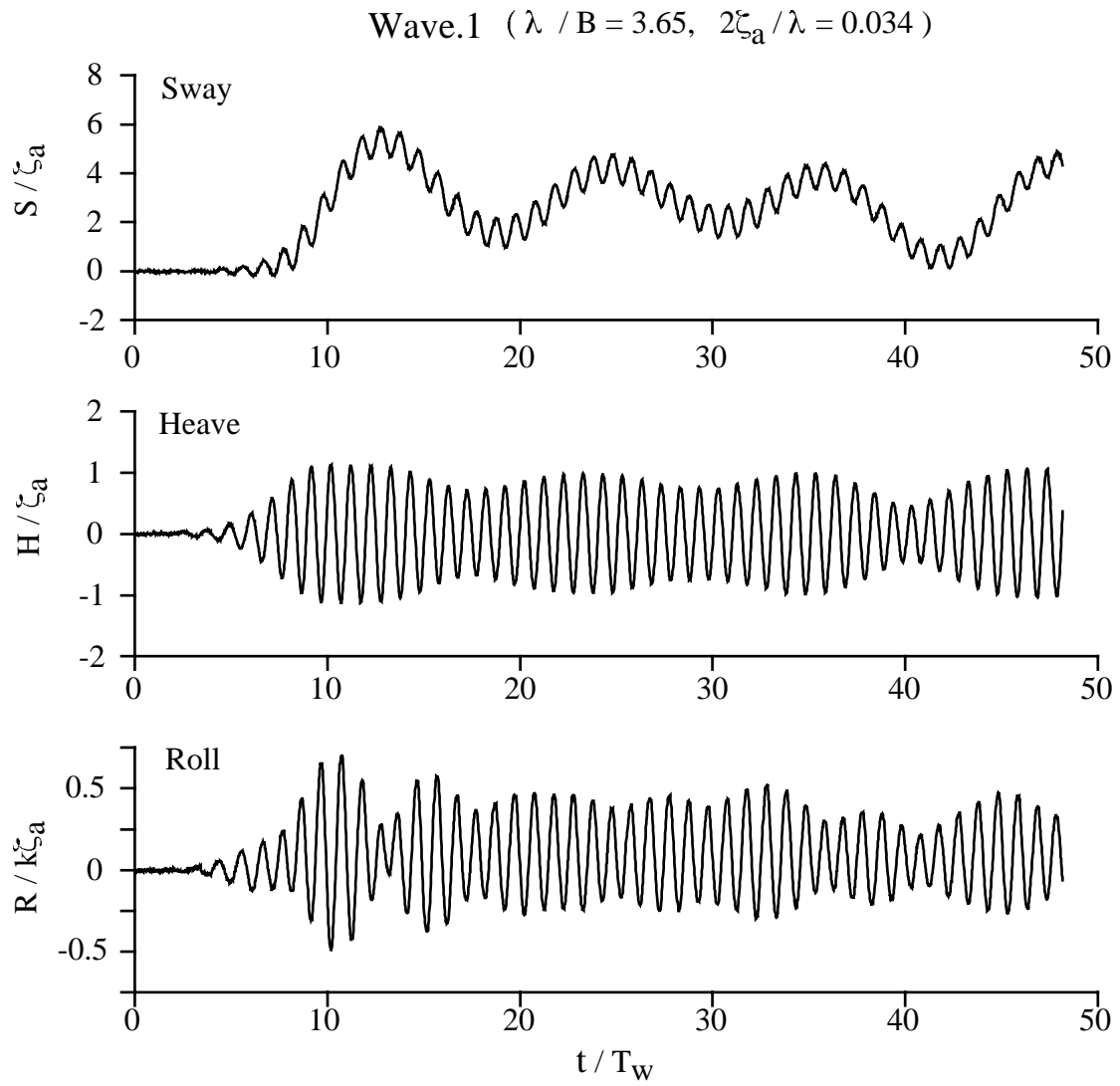


Fig.16: Measured floating body motions in Wave.1

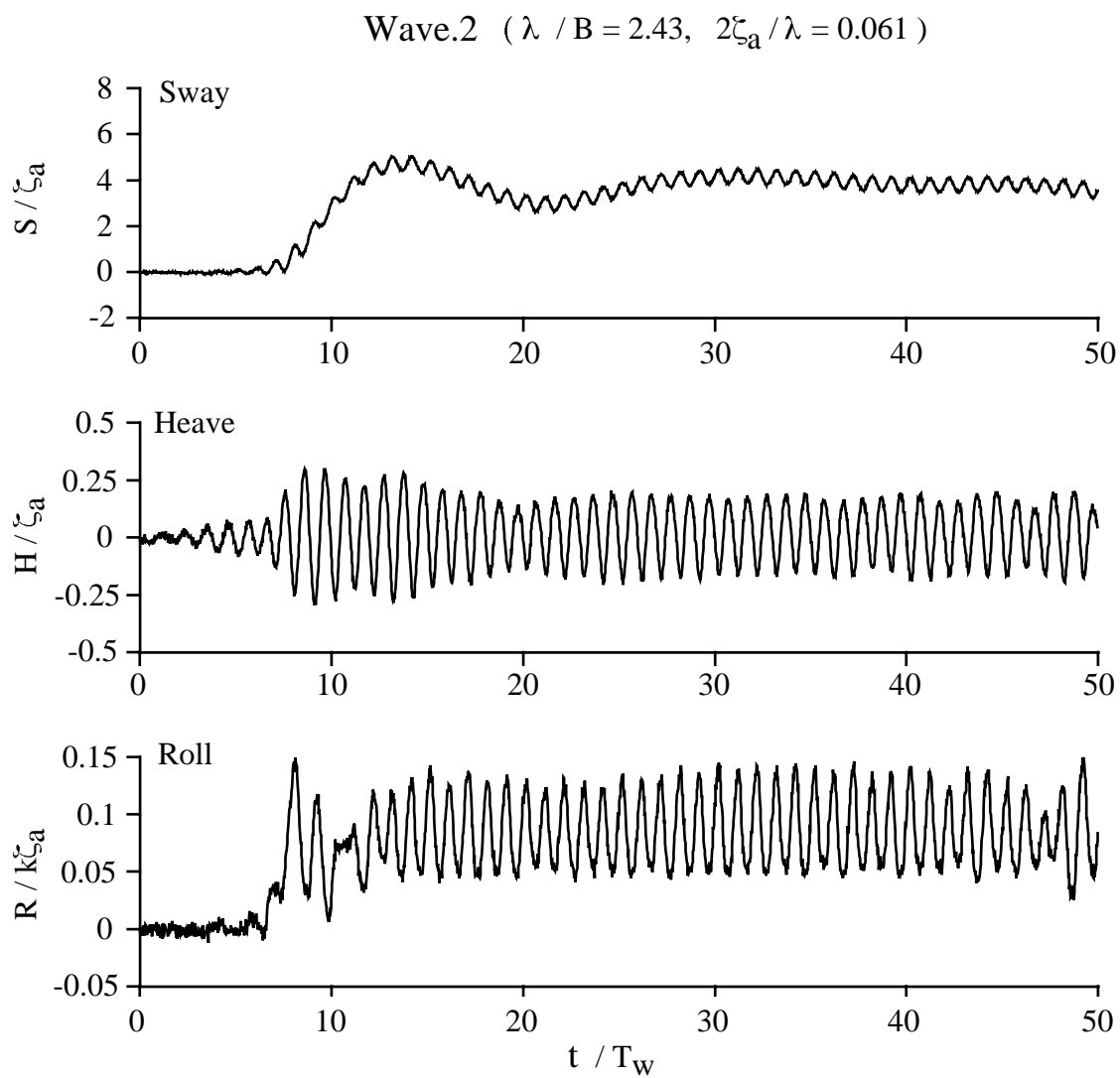


Fig.17: Measured floating body motions in Wave.2

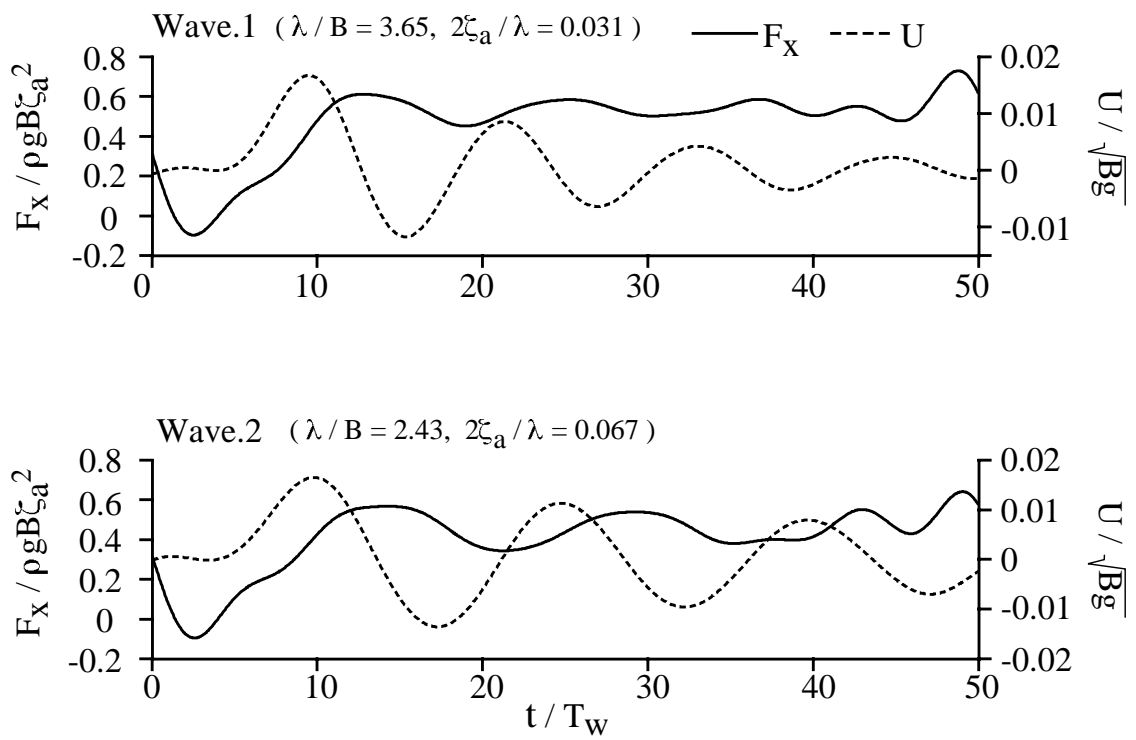


Fig.18: Wave drift force and drifting speed

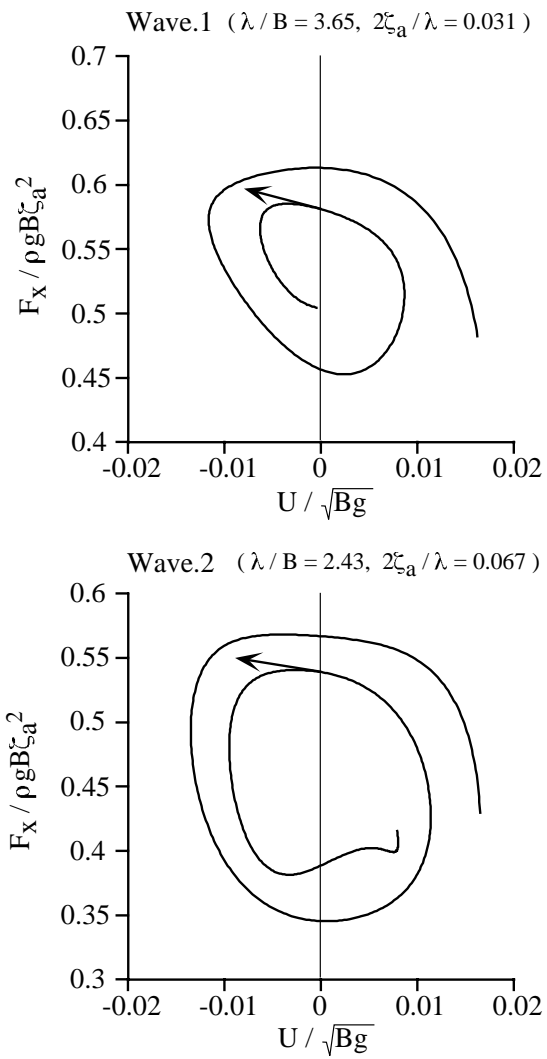
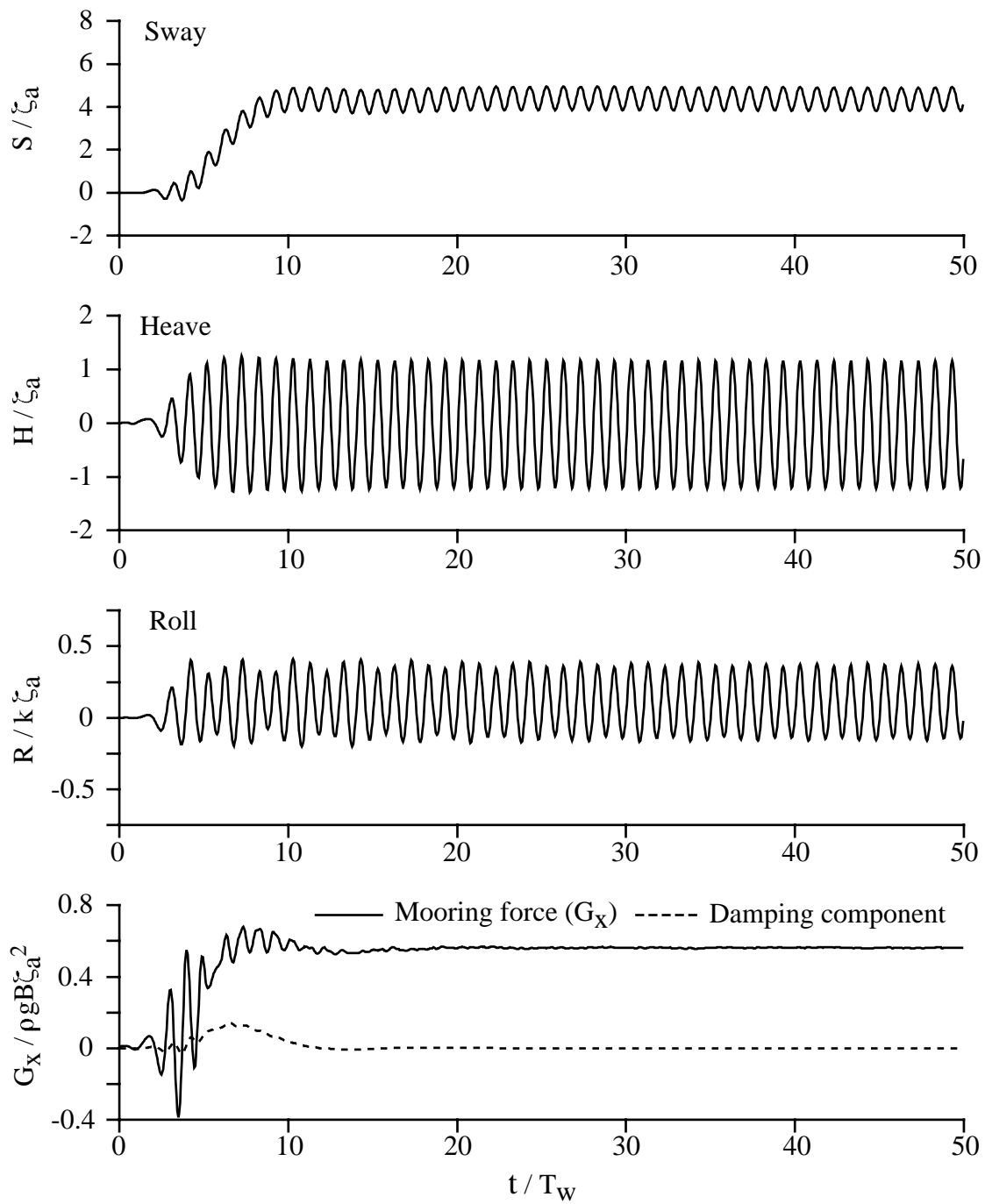


Fig.19: Plot of wave drift force vs. drifting speed



Wave Length  $l = 2.7 \text{ m}$   
Wave Height  $h_w = 2\zeta_a = 10 \text{ cm}$

Fig.20: Simulated floating body motions with the artificial mooring